Iran University of Science and Technology
School of Metallurgy and Materials Engineering

Fabrication of Ti-6Al-4V based scaffold with Mg particles and investigation on its mechanical and biocompatibility properties

A Thesis Submitted in Partial Fulfillment of the Requirement for the Degree of Master of Science in Biomedical Engineering, Biomaterial

By:
Seyed Mohammad Kalantari

Supervisor:
Dr. Shamsodin Mirdamadi
Dr. Hossein Arabi

June 2014

Abstract

Metallic scaffolds have preferably been chosen for bone tissue engineering applications where load-bearing capacities are required. In this project, mechanical properties and biocompatibility of Ti-6Al-4V based composite scaffold with Mg particles were investigated. At first, Ti-6Al-4V powders were prepared by ball milling of machining scraps. The XRD spectrum revealed that the ball milled (prepared) powders were mainly Ti6Al4V. No considerable change has been observed during ball milling so that all diffraction patterns contain only peaks of titanium. After the Ti-6Al-4V and Mg powders (15, 25, and 35 wt%.) were mixed properly, they were compacted into steel die by applying pressure of 500 MPa and sintered in a sealed quartz tube at 900 °C for 2 hours. Employing Archimedes' principle and Image Tool software, total and open porosities of scaffolds were in the range of 46-63% and 24-36%, respectively. The observed ultimate compressive strength of samples was in the range of 72-132 MPa and the Young's moduli were 37-47 GPa. According to mechanical properties results, the sample with 15 wt.% Mg is a good candidate for cortical bone. After 28 days soaking in SBF, the samples with 15, 25, and 35 wt%. Mg indicated 3%, 8%, and 9% mass losing, respectively. SEM and EDS were used for studying the specimen surfaces after immersing for 28 days. The results showed Ca and P deposited within porous areas more than smooth surfaces due to the presence of Mg particles which provoked formation apatite layers. Using atomic absorption spectroscopy (AAS) indicated that by increasing the amount of Mg in scaffolds, calcium concentration of SBF decreased. The biocompatibility of samples were studied by MTT and cell attachment assays. SEM micrographs showed that MG63 cells with normal morphology were able to adhere and proliferate on the surfaces of scaffolds.

Keywords: Ti-6Al-4V scaffold, Mg, Mechanical properties, SBF, Biocompatibility properties

Table of contents

Table of contents III

List of Abbreviations IV

Introduction 1

Materials and method 5

- 2.1. Preparing materials 6
- 2.2. Fabrication of scaffold 7
- 2.3 Pore characterization 9
- 2.4. Soaking in the simulated body fluid (SBF) 9
  - 2.4.1. Characterization of surface morphology 10
  - 2.4.2. Measurement of calcium concentrations and pH 10
- 2.5. Mechanical testing 10
- 2.6. Cell culture 11
  - 2.6.1. Proliferation of osteoblast-like cells 11
  - 2.6.2. Cell morphology 12

Results and discussion 13

- 3.1. X-ray diffraction 14
- 3.2. Characterization of porosity and pores 15
- 3.3 SBF bioactivity 18
  - 3.3.1 SEM & EDS analysis 18
  - 3.3.2. pH value measurement 21
  - 3.3.3 Calcium concentration 22
- 3.3. Compressive behavior 24
- 3.4. In vitro assays 27

Conclusion 31

References 34

List of Abbreviations

Ti	Titanium
MRI	Magnetic Resonance Imaging
PM	powder metallurgy
HA	hydroxyapatite
SEM	scanning electron microscopy
AAS	atomic absorption spectroscopy
ASTM	American Society for Testing and Materials
PVA	polyvinyl alcohol
XRD	X-Ray Diffraction
SBF	simulated body fluid
EDS	energy dispersive spectroscopy analysis
MTT	Dimethylthiazol diphenyl tetrazolium bromide

Chapter 1

Introduction

A biomaterial is a synthetic material used to replace part of a living system or to function in intimate contact with living tissue [1]. A great variety of materials from metals, ceramics and polymers, to composites have been developed and used for medical implants [2]. Table 1.1 summarizes materials commonly used as biomaterials.

Table 1.1 Materials commonly used for biomedical applications [2]

Materials	**Advantages**	**Disadvantages**	**Applications**
Metals: stainless steel, Ti alloys, Co-Cr alloys, Mg alloys, etc.	Though, strong, ductile	Non bioactive	Load bearing implants; dental implants, joint replacement, cardiovascular stents, etc.
Ceramics: zirconia, alumina, bioglass, calcium phosphate, etc.	Bioactive, inert,	Brittle, not resilient	Orthopaedic and dental implants
Polymers: nylon, polylactide, polyethylene, polyesters, etc.	Bioactive, resilient	Not strong	Blood vessel grafts, sutures, hip sockets, etc.
Composites: amalgam, fiber-reinforced bone cement, etc.	Tailor made	Relatively difficult to make	Bone cement, dental resin

Metal implants are required to be non-magnetic and have high density in order to be compatible with magnetic resonance imaging (MRI) techniques and to be visible under X-ray imaging. Most of artificial implants are subjected to loads either static or repetitive, and this condition requires an excellent combination of strength and ductility. This is the superiority of metals over polymers and ceramics [2].

In contrast to the ceramic and polymeric biomaterials which possess poor mechanical properties, metallic biomaterials have been known as the most suitable materials for load-bearing applications [3]. Titanium and its alloys are nowadays the most attractive metallic biomaterials due to their good mechanical properties, unique biocompatibility, and high corrosion resistance among all other metals [4-9]. However, the major limitation concerning metallic implants in orthopedic surgery is the mismatch of elastic module between the bone (0.1–30 GPa) and metallic implants (110 GPa for Ti) following the stress shielding and bone resorption over time [10-15]. One solution to solve this problem in medical applications has been the development of materials that exhibit substantial surface or high total bulk porosity [10].

The fabrication techniques of porous metals are classified into four groups of production: liquid, solid, gas, and aqueous solutions. Due to high activity of titanium with atmosphere gases at molten state, most of the production methods are not adequate [15-17]. Among these methods, the simplest fabrication technique for producing porous metal is powder metallurgy (PM) route which is widely used due to its considerable advantages such as low cost, better control and the capability of near-net-shape production [16].

Pore sizes and shapes obtained in PM are a function of powder size and shape as well as the shape and size of space holder [18]. Conventional space holders are carbamide, sodium chloride, ammonium hydrogen carbonate, and magnesium [3, 16, 18, 19]. Among these space holders Mg could be a good candidate in titanium scaffolds production, since its solubility in titanium is expected to be negligible. Mg has a density of 1.74 g/cm^3, similar to that of natural bone [20, 21]. An adult human has about 30 g magnesium in his body, which most of it existing in muscle and bone. Dietary magnesium deficiency has been identified as a risk factor for osteoporosis [21]. In addition, magnesium binds strongly to phosphates and through its control of hydroxyapatite (HA) (calcium phosphate) formation, influences the mineralization of bony tissue [22]. Furthermore it enhances osteoconductivity of scaffolds if it remains and does not constitute a drawback for biomedical applications [23].

There are two serious consequences of the corrosion process of Mg implants. The first is the formation of hydrogen gas bubbles which appear within one week after surgery and can be easily treated by drawing off the gas using a subcutaneous needle [24]. However, it is reported [25] that hydrogen (H_2) has the properties of antioxidation, anticancer, and anti-inflammatory due to reduce reactive free radicals. An article published in 2007 [26] has suggested that a hydrogen evolution rate of 0.01 $ml/cm^2/day$ can be tolerated by the human body. Thus, it is reasonable to believe that hydrogen gas is not a serious problem. Another undesirable consequence of the Mg and its alloys degradation is rising in pH value. According to Ma Nan et al [25], the pH value had a great effect on the enzymatic activities of superoxide dismutase, peroxidase, and catalase in cells. The high pH value might lead to reduction on activity of these enzymes in cells [25].

In conclusion, employing magnesium as a space holder and its incomplete removal from the scaffold can results to fabrication of porous structure and promotes its biocompatibility, simultaneously.

In this project, firstly, Ti-6Al-4V initial powders were produced by milling scraps of residual machining which hold 40% of initial raw materials used in manufacturing of different parts [27]. Fabrication of Ti–6Al–4V alloy scaffold with different amount of Mg powder volume by powder metallurgy was described. The pore characteristics (pore shape, size, and interconnectivity) were examined using scanning electron microscopy (SEM). Effect of the amount of Mg on bioactivity was determined by immersing samples in SBF and atomic absorption spectroscopy (AAS) was used to measure amount of Ca in solution. Mechanical and biocompatibility properties of these fabricated metallic scaffolds were investigated in this study.

Chapter 2

Materials and method

2.1. Preparing materials

Residual spring-like chips from machining process of Ti6Al4V bars were used as starting material. In order to determine the exact chemical composition of the as-received chips, quantometer analysis was applied on raw Ti6Al4V bar (Table 2.1). A very similar chemical composition was found agreed with the specification for Ti–6Al–4V powders used for coating surgical and medical implants (ASTM F1580-01) [28].

Table 2.1 Mean chemical composition of Ti-6Al-4V bar(wt.%).

Element	**Ti**	**Al**	**V**	**Cu**	**Mo**	**Sn**	**Si**	**Fe**	**Zr**	**Mn**	**C**
Wt.%	88.04	6.33	4.99	0.01	0.02	0.00	0.00	0.48	0.00	0.01	0.77
ASTM F1580-01	Balance	5.5-6.75	3.5-4.5	0.1	-	0.1	-	0.3	-	-	0.8

Since the spring-like chips filled up the most of vial volume, preventing balls to move effectively in milling process, prior to milling chips were manually crushed in a mortar to obtain small pieces with a length less than 1 cm. (Fig. 1.1)

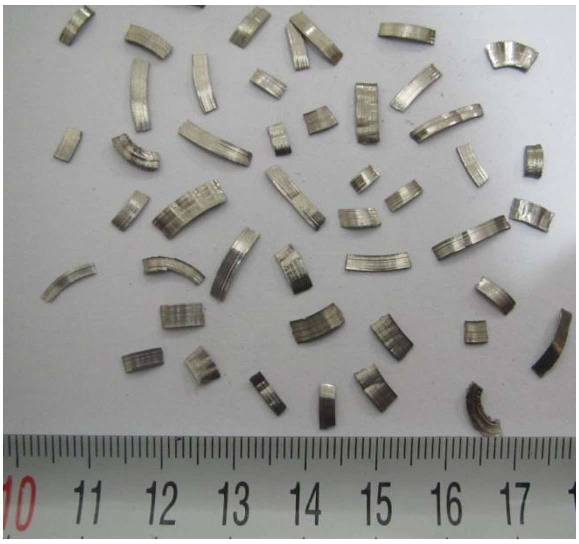

Fig 1.1 Light micrograph of crushed chips before ball milling

Planetary ball milling machine (Retsch PM400 type) under protective atmosphere of Ar (99.998% pure) using) was used to crush chips to much smaller pieces. The powder was ground in a tungsten carbide closed vial. The powder to ball mass ratio was about 1:10 and the rotation speed was maintained at 250 rpm. The milling operation was performed for 6 hours in such a way that the rotary machine was on for 20 min and 10 min off for cooling. Ethanol was added to the vials to act as a coolant and prevent excessive heat generation during ball milling. The crystal structure of the as milled powder was characterized by means of X-ray diffraction (Philips X’PERT MPD) using filtered Cu Ka radiation (k= 0.1542 nm).

2.2. Fabrication of scaffold

Ti-6Al-4V and magnesium (Merck499% pure) powders were sieved separately to obtain a powder range of 37–90µm for the alloy and 90–180µm for Mg powders. Then various amounts of Mg powders (i.e., 30, 45, and 60 vol% Mg) were mixed with the alloy powder in an agate mortar using 5 wt% polyvinyl alcohol (PVA) solution (5 wt% PVAþ95 wt% water) as the binder prior to compaction. PVA solution was required for coating of coarse Mg particles with fine Ti-6Al-4V powders uniformly. Mixing time was determined as 30 min to assure a homogeneous distribution of powders. Then the mixtures were uniaxially pressed at a pressure of 500 MPa in a steel die using a hydraulic press. The heat treatment process consisted of two steps, i.e., at 4501C for 2 h to allow debinding of PVA and then 9001C for 2 h for sintering. Production steps involved in the space holder technique applied are summarized in Fig. 1.2.

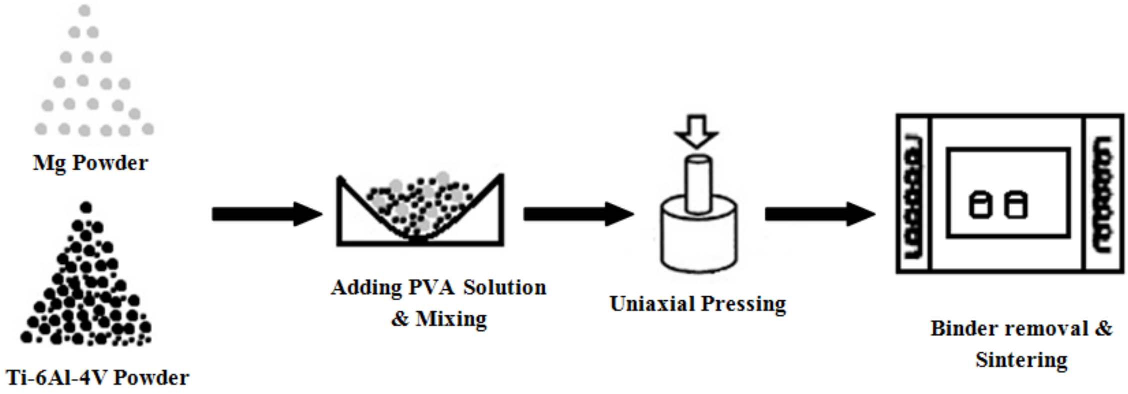

Fig 1.2 Schematic of processing steps for fabricating scaffolds.

Argon flow rate was kept at a minimum adequate to provide a positive internal pressure inside the furnace to avoid possible leakage of air into the furnace. Samples were placed in a quartz tube in order to reduce evaporation of magnesium. The main phases in the scaffold were identified by X-Ray Diffraction (XRD Philips X'PERT MPD) analysis using a Cu-Kαradiation source. To reduce evaporation of Mg, samples were placed in a quartz tube as shown in Fig 1.3.

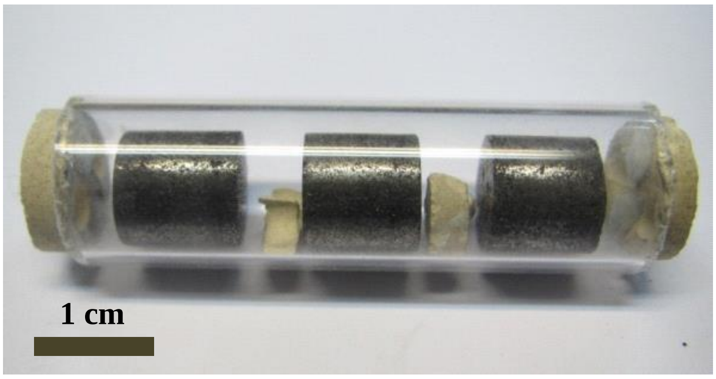

Fig 1.3 Samples in a quartz tube in order to reduce Mg evaporation.

2.3 Pore characterization

Porosity contents of the porous Ti-6Al-4V/Mg samples were determined via Archimedes' principle. The pore morphology and interconnectivity were observed using scanning electron microscopy (SEM, TESCAN VEGA//XMU). Some of the characteristics (i.e. size distribution, and roundness) were evaluated by image analyzer attached to an optical microscope and suitable analysing software (Image Tool). For the image analysis, the sectioned parts were prepared by a sequence of conventional metallographic steps.

2.4. Soaking in the simulated body fluid (SBF)

Before soaking the samples in SBF, their surfaces were polished with 600# grit silica papers and washed ultrasonically in acetone, alcohol and deionized water for 15 min. The sintered compacts were then immersed in SBF for up to 4 weeks to access its bioactivity. SBF is prepared by dissolving reagent grade NaCl, KCl, $NaHCO_3$, $MgSO_4.12H_2O$, $CaCl_2$ and KH_2PO_4 into distilled water and buffered at pH = 7.4 with tris-hydroxymethyl aminomethane (TRIS) and HCl at 37 ºC according to reference [29]. The ion concentration of the SBF is shown in Table 2.2.

Volumes (Vs; ml) for the immersion liquid were calculated based on the formula: $V_s=10/S_a$ where S_a (cm^2) was the surface area of each samples.

Table 2.2 Comparison of the ionic concentration in blood plasma and the theoretical one in SBF (mmol/l) used in this research [29].

	Na^+	K^+	Mg^{2+}	Ca^{2+}	Cl^-	HCO_3^-	HPO_4^{2-}	SO_4^{2-}
Blood plasma	142.0	3.6-5.5	1.0	2.1-2.6	95.0-107.0	27.0	0.65-1.45	1.0
SBF	142.0	5.0	1.0	2.5	126.0	10.0	1.0	1.0

2.4.1. Characterization of surface morphology

Specimens were taken out from the SBF after 28 days. Changes in the surface structural of the specimens were observed after immersing them in SBF for a certain time. These surfaces were characterized by scanning electron microscopy (SEM TESCAN VEGA//XMU) with energy dispersive spectroscopy analysis (EDS).

2.4.2. Measurement of calcium concentrations and pH

Changes in the concentrations of calcium element in the SBF due to the immersion of the specimens were determined by atomic absorption spectroscopy (AAS GBC-Avanta ∑) technique after 2,9,18 and 28 days. Changes in the pH value of the fluid were also measured during 18 days. The SBF, in which the specimens for surface examination were immersed, was refreshed every two days. However the SBF used for measuring pH and calcium concentration was not refreshed throughout the whole observation process.

2.5. Mechanical testing

Compression tests were carried out on the scaffolds with a size of φ 10×10 mm^2 at ambient temperature (25 ◦ C) at a constant cross-speed of 0.5 mm/min^{-1} employed(by using) Instron-1185 universal test machine. Three specimens were tested in each porosity level to compensate the possible scattering of the results (For each ratio of starch to titanium, three samples in the same range of porosity were fabricated, and all of them were used for compression testing). The elastic moduli of the specimens were calculated from curves fitted to the linear elastic regions of the stress strain curves while yield strengths of the sintered samples were calculated using the 0.2%-offset method

2.6. Cell culture

Prior to cell culture, the porous samples were cleaned and sterilized in order to create a clean surface for cell proliferation. Each sample was cleaned ultrasonically in acetone, 100% ethanol and deionized water for 15 min. They were then dried with a hair-dryer and subsequently autoclaved at 121 °C under a pressure of 1.5 Kg/cm2 for 1 hour before placing them in multiwell culture plates.

Osteoblast-like MG-63 cells (NCBI C-555, National Cell Bank of Iran, Pasteur Institute of Iran) were cultured at a density of 1×10^4 cells on each sample. MG-63 cells were cultured in Dulbecco's Modified Eagle's Medium (DMEM; GIBCO, Scotland) supplemented with 10% fetal bovine serum (FBS, Gibco), 100 U/mL penicillin, and 100µg/mL streptomycin (Sigma, U.S.A.). MG-63 cells were harvested with 0.25% trypsin-EDTA solution (Sigma) in phosphate buffered saline (PBS, pH 7.4). According to the ISO 10993-5, osteoblast-like cells were incubated at 37 °C in humidified air with 5% CO2. The cultured medium was changed every two days.

2.6.1. Proliferation of osteoblast-like cells

Dimethylthiazol diphenyl tetrazolium bromide (MTT) assay was used for evaluation proliferation rate of osteoblast cells. Briefly, MG-63 cultured cells were resuspended in culture medium at a density of 1×10^3 cells/50 µL and were added to each of the wells in the 96-microtiter plates (NUNC, Denmark).The plates were incubated at 37 °C in a humidified atmosphere of 5% CO2 in air for 24 h. The scaffolds with different weight percent of magnesium were placed on the MG-63 cells. One tissue culture polystyrene (TPS) well used as a control. The plates containing scaffolds and the cells were incubated at 37°C with 5% CO2 for 7 days. Every three days, cultured medium was changed. At predetermined intervals, scaffolds were taken out of wells. 100 microliters of MTT (5 mg/mL in medium) was added to each of the wells and incubated for another 4 h at 37 °C in a humidified atmosphere of 5% of CO2 in air. At this stage the MTT was removed and the formazan crystals were dissolved by adding 100 µL of isopropanol (Sigma) in each well. The plates were placed in the incubator for 10 min and then in a cold room for 15 min prior to absorbance measurements. Multiwell microplate reader (ICN, Switzerland) was used for reading optical density (OD) of each well at 545 nm wavelengths. The experiment was repeated three times.

2.6.2. Cell morphology

Morphology of cells which are attached to samples was studied using SEM. MG-63 cells at a density of 5×10^3 cells/well in 24-well plates were placed on each scaffolds. The plates were incubated at 37 °C in humidified air containing 5% CO2. 2.5% glutaraldehyde buffered in 0.2 M phosphate-buffered saline (PBS) was used for fixing cells after 72 h of incubation period. Graded alcohols (50, 70, 90, 95, and 100%) were used for dehydrating specimens. Dehydration was carried out by air drying for 24 h. The specimens were observed using SEM after sputtering a gold layer.

Chapter 3

Results and discussion

3.1. X-ray diffraction

The result of X-ray diffraction of ball milled alloy powder is presented in Fig.3.1.

The XRD spectrum reveals that the ball milled powders were mainly Ti6Al4V. No considerable change in the position of peaks was observed after ball milling such that all diffracted peaks are related to Ti-6Al-4V. Additionally, neither oxides nor nitrides were detected although titanium is very reactive element and prone to form various oxides and nitrides such as TiO, TiO_2, Ti_2O_3, Ti_3O_5, TiN, when it is in contact with oxygen, water vapor, air and nitrogen gas. In comparison to the use steel container and steel ball which induce Fe contamination [27], when tungsten carbide vial is used no intermetallic compound formed during ball.

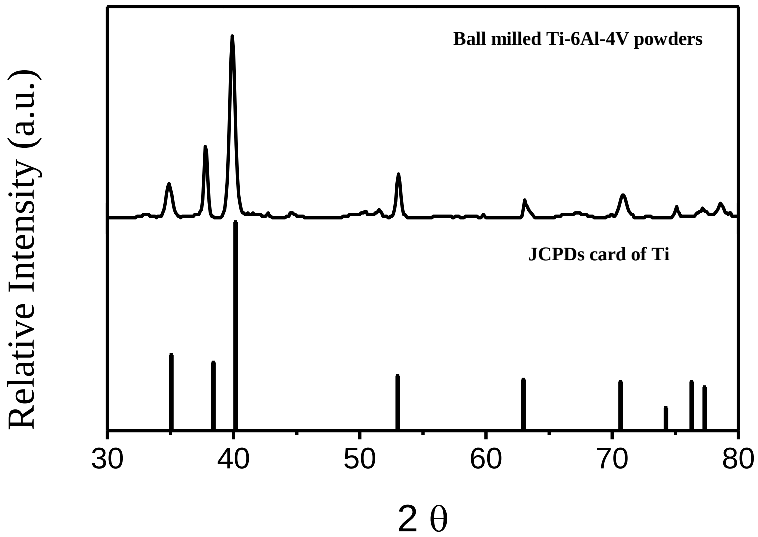

Fig 3.1 The results of X-ray analysis for the prepared Ti-6Al-4V powders, together with the JCPDs card for Ti.

3.2. Characterization of porosity and pores

The results of the image analysis for specimens are summarized in Table 3.1.

The open porosity is expressed as a percentage of the interconnected pore space in total porosity. Image analysis indicated that total porosity and open porosity tend to increase from 47% and 41% to 64% and 47%, respectively, with increasing the amount of magnesium. Porosities in the scaffolds that manufactured by partial evaporation of magnesium were basically open type pores.

Table 3.1 Pore characterizations extracted from software Image Tool and use of Archimedes' principle.

Sample	Total porosity (%)	Open porosity (%)	Roundness (%)
Ti6Al4V/30Mg	47±6	41±8	25
Ti6Al4V/45Mg	54±5	43±6	22
Ti6Al4V/60Mg	64±10	47±13	28

According to Fig. 3.2, two types of pores remained after sintering. One was the small pores having several micrometers mean diameters were inherited from the space among Ti6Al4V particles after compaction while the large pores were generated after the partial evaporation of magnesium.

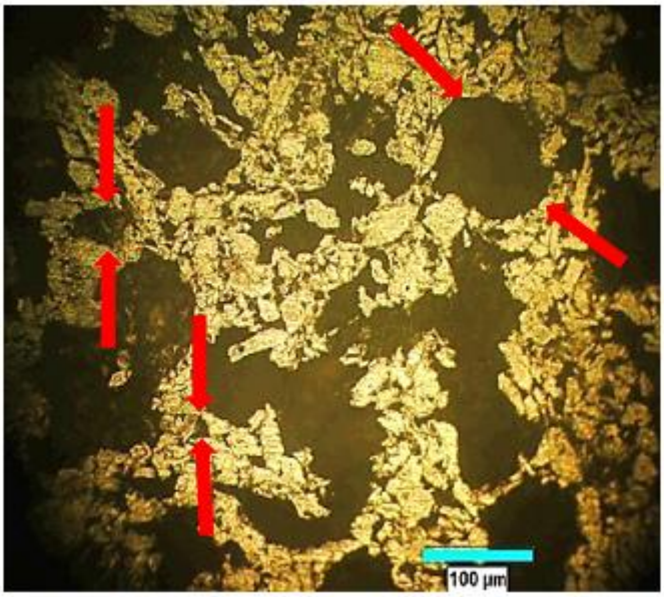

Fig 3.2 Micro and macro pores after the partial evaporation of Mg from scaffold.

The pore size and shape were a function of the size and shape of prime powders used. Typical pore morphologies of the scaffolds surfaces having different amounts of magnesium are presented in Fig. 3.3.

Distribution of large pores in various samples can be seen in Fig. 3.3. Their shapes are irregular and have different sizes due to the irregular shape and inconsistent sizes of Mg particles. As the total porosity of the compacts increased, the average roundness of pores also increased mainly due to inter-connection of macropores at higher porosity levels which was found to be 28% for sample having 64% porosity. It should be noted that compacts having greater than 20 vol.% porosity are considered as promising samples for biomedical applications since it has reported [30]the optimal porosity of implant materials for ingrowths of new-bone tissues is in the range of 20–50 vol.%. The pore size distributions of scaffolds are shown in Fig. 3.4.

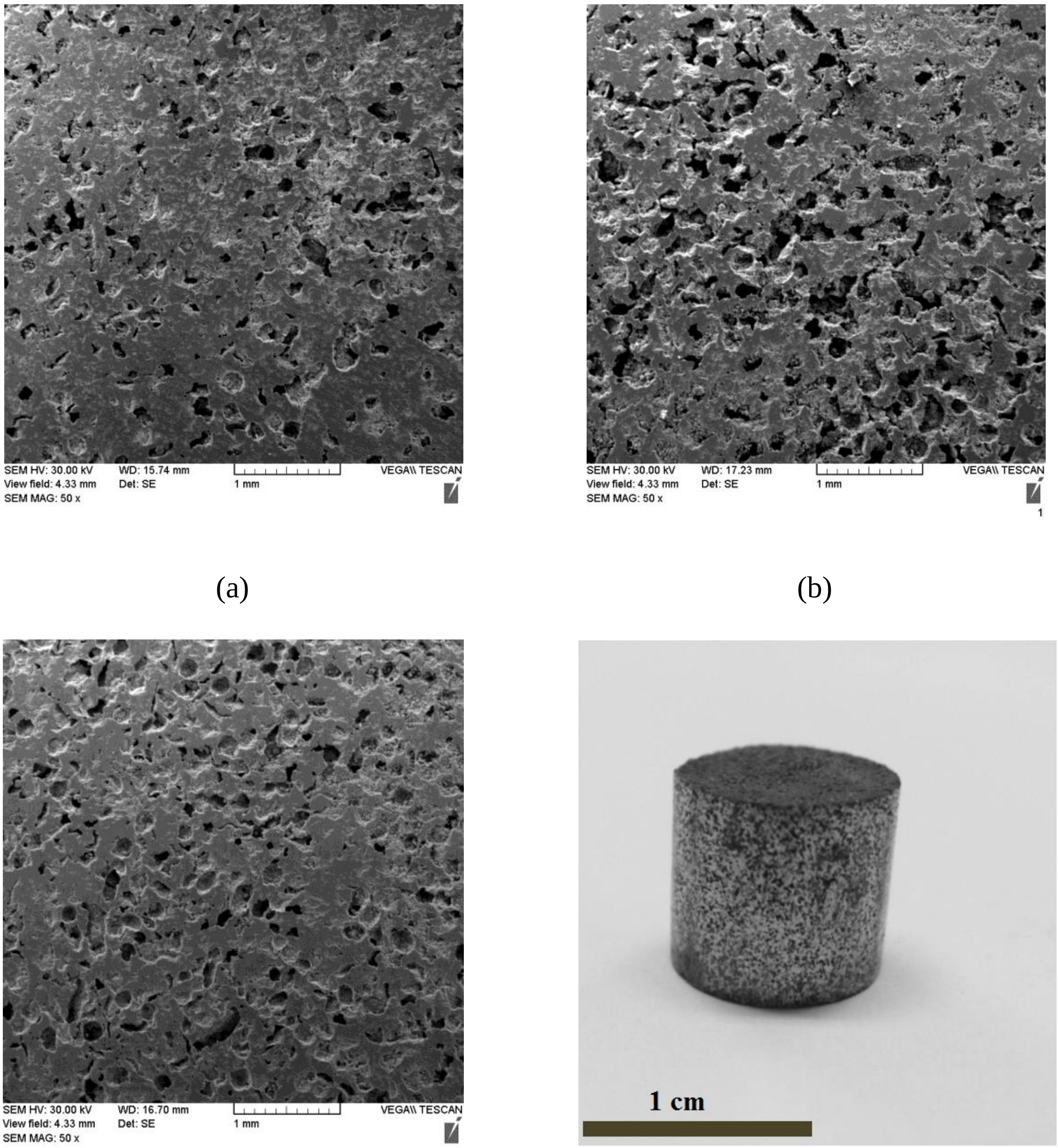

(a) (b)

(c) (d)

Fig 3.3 Pore morphology in Ti-6Al-4V scaffolds surface having: (a) 30, (b) 45, and (c) 60 vol.% Mg. A typical Macrophoto of the Ti-6Al-4V/Mg scaffold can be seen in (d).

The data presented in Fig. 3.4 show that the pore size distributions are mainly in the range of 20-60 µm, and higher ranges obtained in the samples with higher magnesium content. This phenomenon can be explained by considering the area of interconnected sites among Mg granules. As these areas decreased, the initial content of Mg decreased and caused a decrease in the pore size. However according to Bobyn et al. [31] and Itala et al [32], the sizes of pores generated due to sintering and partial evaporation of Mg are large enough for the consistent ingrowth of new bone within the porous space.

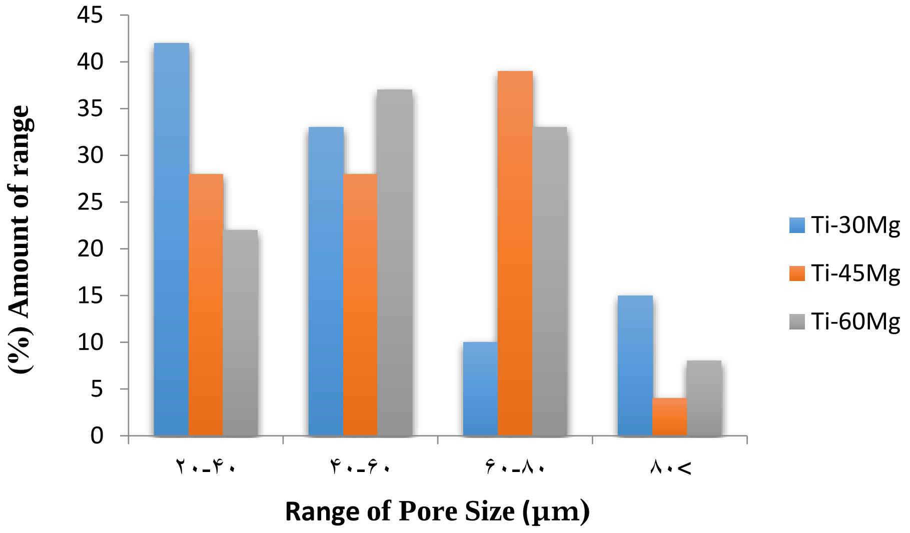

Fig 3.4 Pore size distributions for the porous Ti6Al4V scaffolds produced having various initial Mg contents of 30, 45, and 60 vol.% .

3.3 SBF bioactivity

3.3.1 SEM & EDS analysis

Typical topographies of the specimen's surfaces with 30 and 60 vol.% Mg after immersing in the SBF for 28 days are shown in Fig. 3.5. The SEM micrographs in this figure show a thin layer of Ca and P deposited on the surfaces. After 28 days of immersion, the surfaces of these samples were analyzed by EDS and the results are presented in Figure. 3.6.

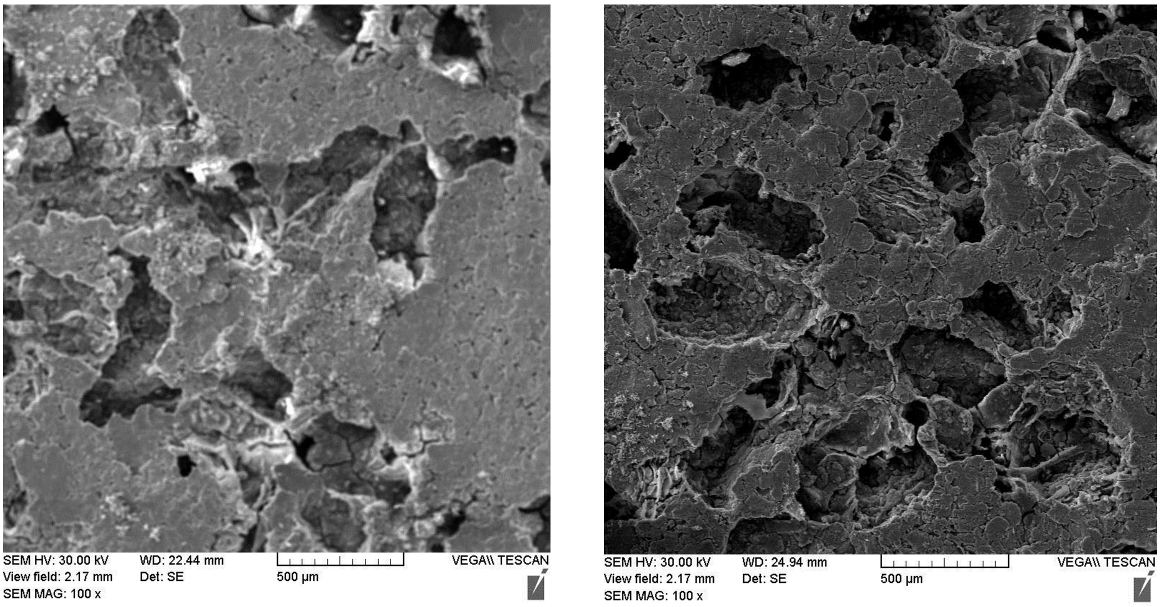

(a) (b)

Fig 3.5 SEM micrographs of the scaffolds surfaces with (a) 30 and (b) 60 vol.% Mg after immersion in the SBF for 28 days.

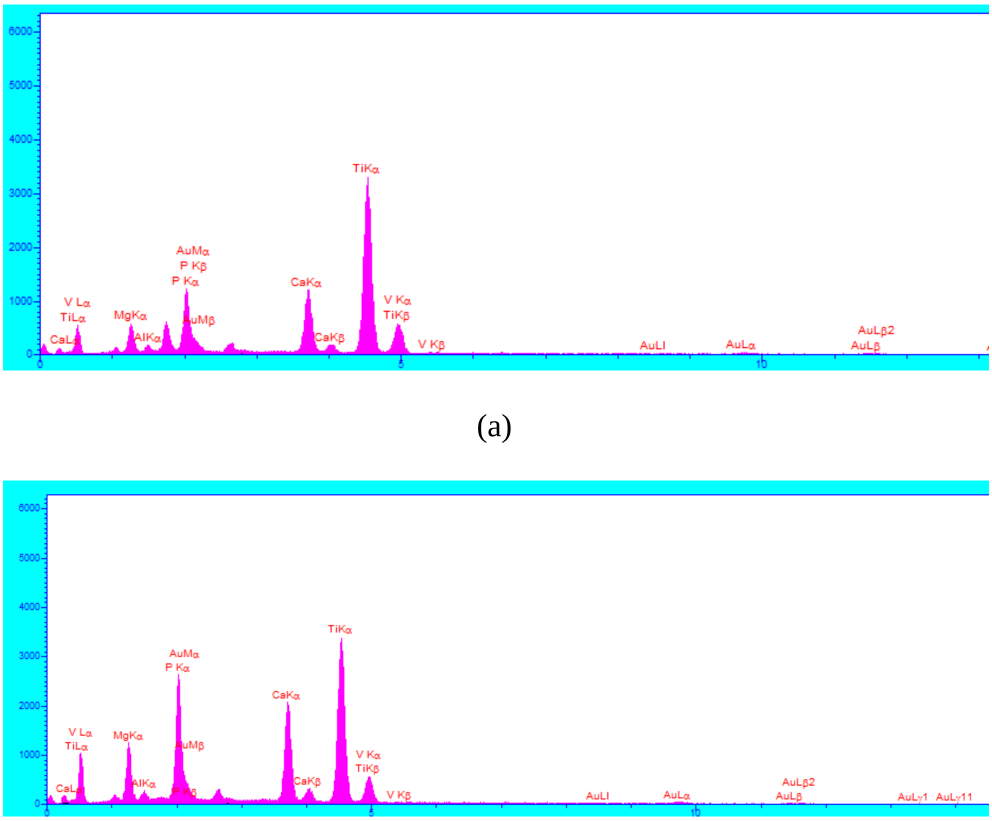

(a)

(b)

Fig 3.6 EDS analysis of the scaffolds surfaces having (a) 30 and (b) 60 vol% Mg after immersion in the SBF for 28 days.

These spectrographs show by increasing the Mg content, the quantity of deposited Ca and P increased. Typical distribution of calcium and phosphorus on the surface of one of the sample is shown in Fig. 3.7. The amount of Ca and P deposited into the porous areas are more than those deposited on smooth surfaces which resulted to an increase in biocompatibility property in pores. Worth mentioning that the prime cause of more Ca and P depositions in pores surfaces can be attributed to the presence of more Mg which caused the formation of large number of porosity due to its partial evaporation during sintering

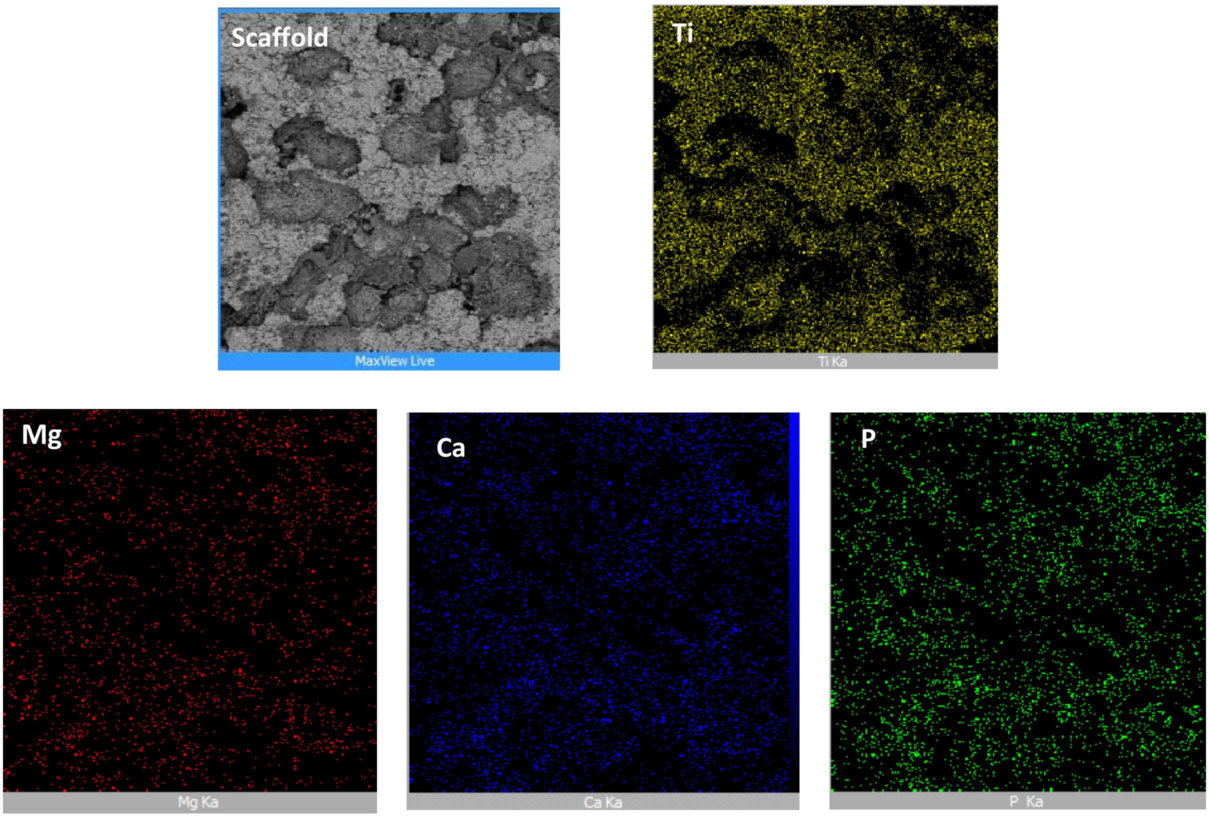

Fig 3.7 Distribution of calcium and phosphorus on the surface of scaffold after 28 days immersion in the SBF for the sample having 60 vol.% Mg.

3.3.2. pH value measurement

Changes occurred in the pH values of the SBF, as a function of immersion time, are given in Fig. 3.8.

The pH values increased gradually throughout the immersion process. The pH values after 18 days were 8.76, 8.96, and 9.06 for specimens by increasing the Mg content from 30 to 60 vol.%. Corrosion of Mg in an aqueous physiological environment can be expressed by the following equations. The primary anodic reaction is expressed by the partial reaction presented in equation (1); at the same time the reduction of protons is expressed by the partial reaction occurring on the cathode and can be presented by equation (2).

Anodic reaction: $\mathrm{Mg} \rightarrow \mathrm{Mg}^{2-} + 2\mathrm{e}^{-}$ (1)

Cathodic reaction: $2\mathrm{H}_2\mathrm{O} + 2\mathrm{e}^{-} \rightarrow 2\mathrm{OH}^{-} + \mathrm{H}_2$ (2)

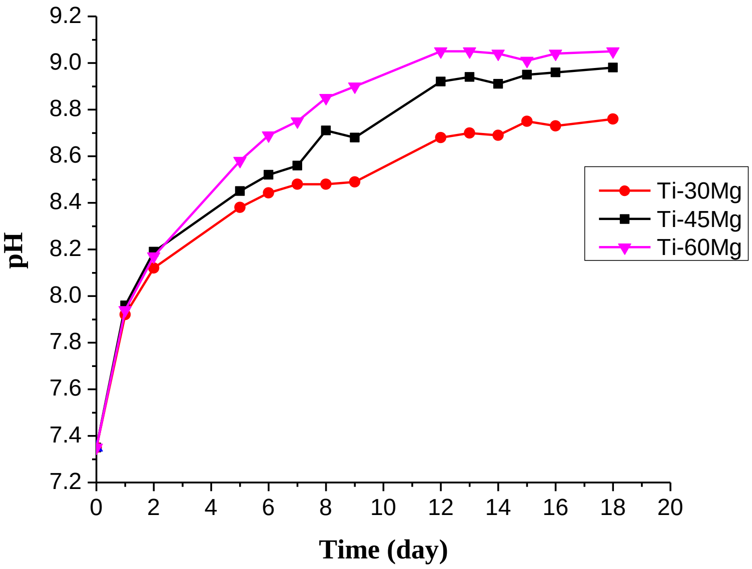

Fig 3.8 Changes in pH value of the SBF as a function of immersion time.

Along the progress of corrosion reaction, pH of the solution near the Mg surface can be increased with the accumulation of OH^{-}, resulting in the precipitation of the $\mathrm{Mg(OH)_2}$ on the surface, because the solubility of $\mathrm{Mg(OH)_2}$

decreases with the increase of OH^- concentration. It has been reported[18][24] that accumulated $Mg(OH)_2$ layer on the Mg surface can act as a barrier against dissolution by preventing mass diffusion between the magnesium substrate and the solution. Therefore, this fact suggests that the accumulated $Mg(OH)_2$ layer on the scaffold surface retarded the Mg^{2+} release after near 12 days. Recently, Robinson et al. [33] reported the novel antibacterial properties of Mg metal against Escherichia coli, Pseudomonas aeruginosa and Staphylococcus aureus. In addition Ma Nan et al [25] have stated that, the pH value has a great effect on the enzymatic activities of superoxide dismutase, peroxidase, and catalase in cells. Therefore the high pH values might lead to reduction on activity of these enzymes in cells. However as reported in reference [34] such extensive changes in pH would not be expected in vivo due to corrosion products can be easily evacuated from the implantation site by lymphatic circulatory systems and the buffering action of the tissue fluid.

3.3.3 Calcium concentration

The calcium concentration as a function of immersion time is shown in Fig. 3.9.

Fig. 3.9 indicates that by increasing the immersion time in SBF, calcium concentration of this solution decreases gradually. The nucleation and growth of the apatite on the porous surfaces consume calcium and phosphorus in the solution resulting to calcium reduction in the SBF. The pH values increased with increasing the mass fraction of magnesium. This increase can easily reach two pH units which leads to a 10–100-fold decrease of HA solubility, and accordingly, a very large acceleration of apatite nucleation according to Bohner et al [35]. Kuwahara et al. [36] declared that the corrosion products on the surface of Mg immersed in Hank’s solution might be amorphous and complicated in their structure. They reported the formation of a compound such as $(Ca_{0.86}Mg_{0.14})_{10}(PO_4)_6(OH)_2$. Considering the similar ion concentrations in the SBF used in this study to those in Hank's solution [36], there might be some amorphous phosphates containing magnesium/calcium in this study. According to Jonasova et al [37], the solution with ions such as PO_4^{-3} ,Ca^{+2} etc, HA is likely to nucleate and grow on the magnesium surface due to the supersaturated condition at high pH. Moreover, when Mg^{2+} ions dissolve into the solution, phosphates containing Mg/Ca form and tightly attach to the matrix. In general, the reaction among $H_nPO_4^{(3-n)-}$, Ca^{+2} and Mg^{+2}could be described primarily as:

$$H_nPO_4^{(3-n)-} + Ca^{+2} + Mg^{+2} + OH^- \rightarrow Mg_xCa_y(PO_4)_z$$

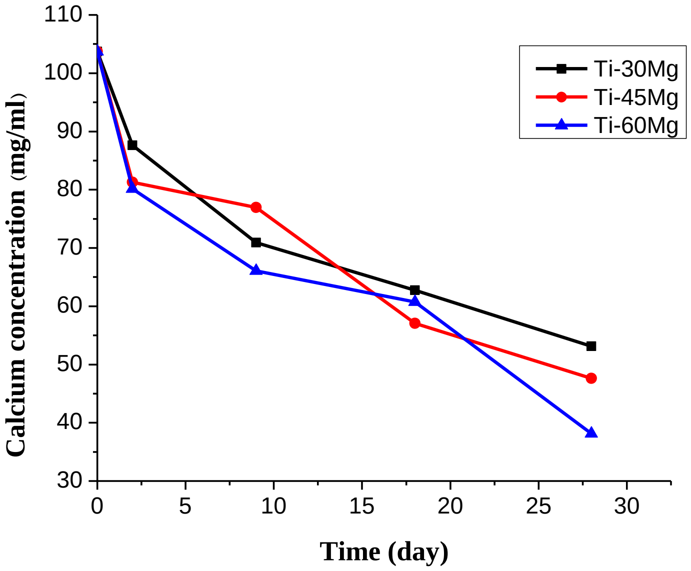

Fig 3.9 Changes in Calcium concentrations as a function of immersion time.

Taking the excess OH- into consideration, some researchers reported [38] that complicated compounds [represented by MgxCay(PO4)z(OH)] might be deposited on the surface .Xu et al [39] also reported that the corrosion layer containing such magnesium-substituted calcium phosphate compounds on Mg can promote osteoinductivity and osteoconductivity, predicting good biocompatibility of magnesium.

3.3. Compressive behavior

Fig. 3.10 presents typical compressive stress–strain curves of the scaffolds having different amounts of porosities.

Compressive properties of the scaffolds are summarized in Table 3.1. Obviously, the compressive strength and Young’s moduli of the samples are inversely correlated with the porosity level. The scaffolds with approx. 47, 54, and 64% porosity exhibited, the compressive strength of 132, 96, and 72 MPa and Young’s modulus of 47, 41, and 37 GPa, respectively. The compressive stress-strain curves exhibited reasonably large total amounts of strains. However the linear strains in all of the samples are low and failed in pseudo-brittle mode which is the major problem of these fabricated Ti-6Al-4V scaffolds. The embrittlement of porous samples might be attributed to the sintering temperature. According to Gagg et al [40] when the temperature of sintering is low and very close to the α to β phase transition point (i.e. 882 °C) formation of brittle ω phase has been observed. This phase prevent enough consolidation between adjacent particles and promote brittle behavior [41]. Furthermore due to weak interface bonding between Mg and Ti-6Al-4V particles and no information of intermetallics, they have no effect on the mechanical properties of the scaffolds [42].

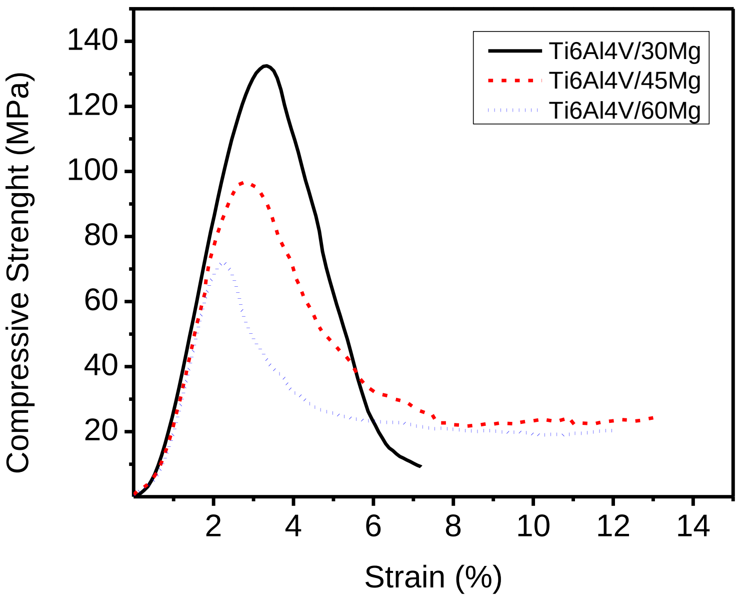

(a)

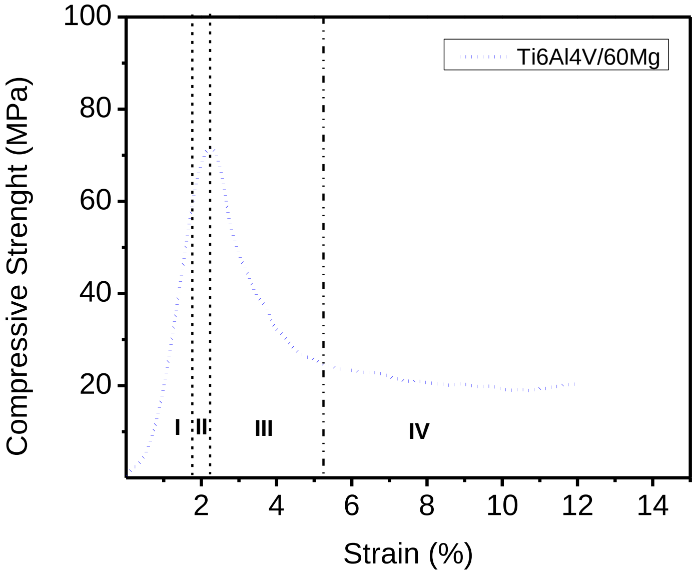

(b)

Fig 3.10 (a) Typical compressive stress versus strain of the porous Ti-6Al-4V scaffolds produced with various initial Mg contents (30, 45, and 60 vol.%.), (b) The Compressive stress-strain curve of scaffold having 60 vol.% Mg with four different deformation regions.

Table 3.1 Mechanical properties of porous Ti-6Al-4V samples tested in compression. The values given together with the standard deviations are average of three tests.

sample	Young's module (GPa)	Compression Strength(MPa)
Ti6Al4V/30 vol.% Mg	47 ± 3.12	132 ± 9.56
Ti6Al4V/45 vol.% Mg	41 ± 2.92	97 ± 6.84
Ti6Al4V/60 vol.% Mg	37 ± 2.31	72 ± 5.14

A typical compression stress–strain curve of the specimens can be divided into four distinct deformation regions marked as I, II, III, and IV on Fig. 3.10(b). In region I, the compact is elastically compressed up to about the proportional limit at the beginning of deformation. According to observations of Tscdemirci et al [43], after the proportion limit and before maximum compressive strength, shear bands starts to propagate along the diagonal axes of the scaffolds at 45° to the compression direction. In this region inelastic deformation under normal and shear forces begins to become non-uniform. In region III, reduction in the load carrying capacity takes place as a consequence of deformation localization in the shear bands. In region IV, fluctuation of stress values occurs around a constant stress as a result of shearing the two cone apices on top of each other (Fig.3.11) according to Tasdemirci et al [43]. Particle separation along the diagonal axes beginning from the corners of the cylindrical scaffold at strains of about 12% leads to complete failure.

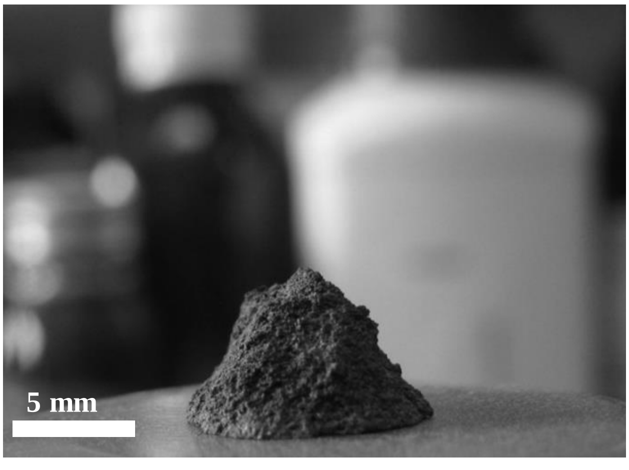

Fig 3.11 The typical ruptured section of compressed sample with the inverse V-shape.

In the present study, the constant stress in region IV has not been observed in scaffold with 30 vol.% Mg, while this region appeared in the other two samples, Fig.6. Therefore, scaffold with 30 vol.% Mg and 47% porosity appears to be appropriate for cortical bone replacement applications not only for its lower strain but for its higher elastic modulus. Scaffolds with greater porosities, on the other hand, seems not to be suitable for load bearing biomedical applications due to their insufficient strengths and higher elongation. Therefore, all the samples exhibited considerably higher strain than 7% are seem to be suitable for cancellous bone according to Aydogmus et al [23].

3.4. In vitro assays

The cell attachment of the MG-63 cells on the surfaces of samples was observed by SEM. SEM images of the extent of cell ingrowth into the porous Ti-6Al-4V structures (Fig. 3.12) showed that a different amount of Mg are associated with different pores, so the more the volume percentage of the pores with higher Mg content, the more will be the extent of the cell ingrowth, helping the formation of bridge across the pores.

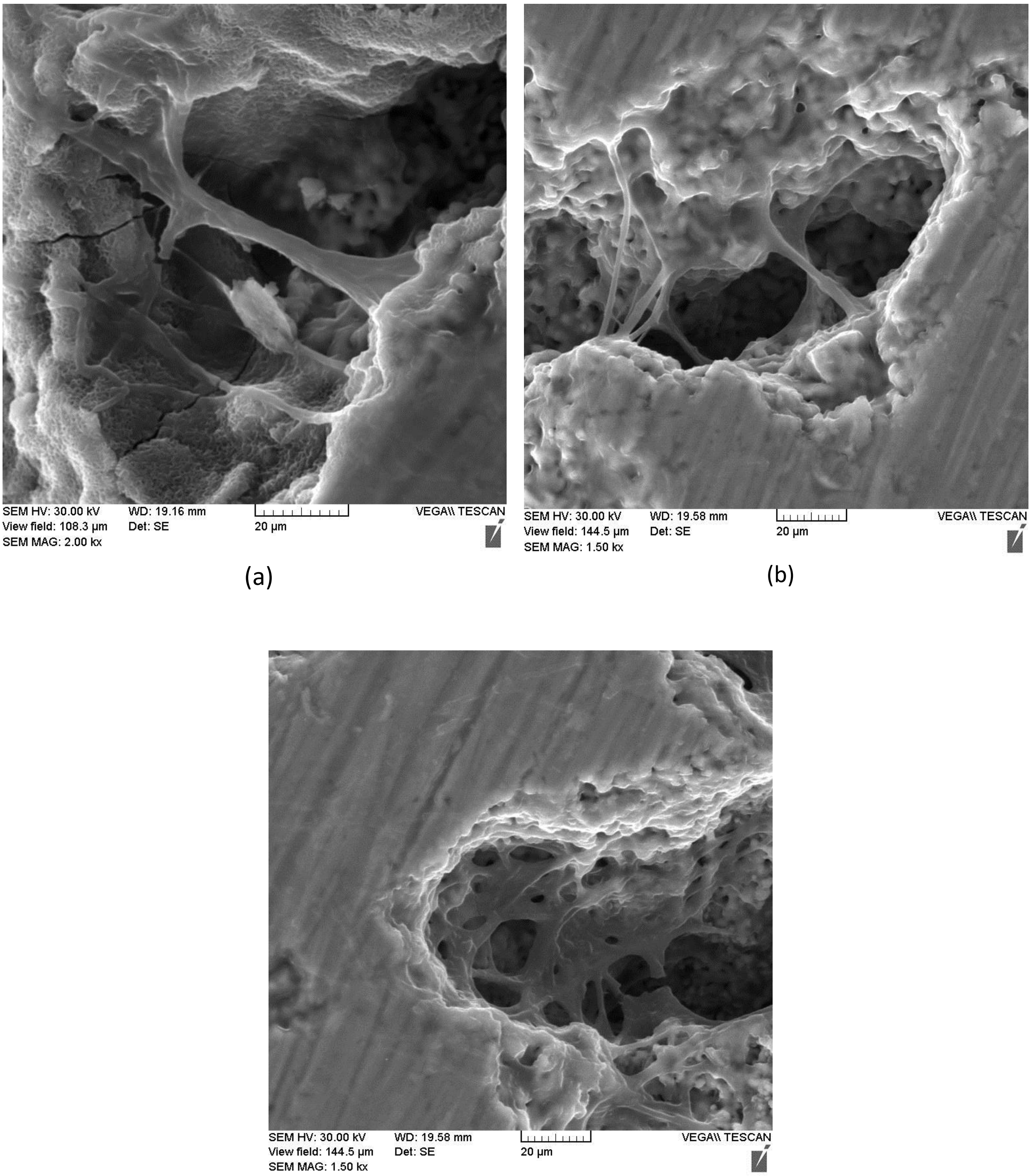

(a) (b)

(c)

Fig 3.12 SEM micrograph of MG-63 cells attached to the scaffold's surface having: (a) 30, (b) 45, and (c) 60 vol.% Mg after 6 h.

It is thought that the membrane-associated adhesion receptors which belong to the integrin superfamily play a crucial role in mediating cellular interactions between osteoblasts and the biomaterial surface [44]. Functional integrins are transmembrane heterodimers consisting of non-covalently associated α and β subunits [45]. Some divalent cations such as Mg^{2+}, Ca^{2+} ,Mn^{2+} could bind motifs which are a part of the extracellular domain of the-subunit and integrin affinity to their respective ligands will be modified due to extracellular changes in these ions [44]. Thus in the presence of Mg within the pores, cells were frequently observed to spread on the surfaces of the particles and bridge the pores as it can be seen in Fig. 3.12.

The cellular behavior is affected by porous materials due to various factors such as pore size. The effect of pore size on cell ingrowth and bridging can be described by hypothetical mechanism presented by Chen et al [46]. They stated that cells prefer to spread on both sides of the gaps between the particles, when a gap is too wide for one cell to bridge. Such attached cells provide closer surfaces for new born cells to attach on it and bridging the gap will be much easier. This process might take place again and again to cover a wide gap by new born cells which bridged by touching the ligands of existing cells. In contrast to wide gap which takes a lot of time for cell bridging and ingrowth, for a narrow gap, the initial attached cells are able to bridge the gap resulting in faster subsequent cell spreading and also leads to faster coverage of the pores by new cells.

Thus it is obvious that pore size is one of the most important factor which affects cell attachment. In 2007 Xue et al [47] declared that human osteoblasts could only bridge pores smaller than 200 µm. Recent studies[30] have shown that pores with smaller size could be beneficial to osteoblastic attachment, proliferation and differentiation. It has been reported [48] that MG63 cells with a diameter of 30 µm has the ability to stretch well in the pores having a size of about 30 µm. In fact it is easier for cells to migrate and settle into the pores with the size equal to itself [48]. It can be observed in Fig. 3.12, where the diameter of pores are less than 30 μm, MG-63 cells exerted good stretching ability and bridged the pores.

The results of MTT assay after 7 day incubation are shown in Fig. 3.13. Viability percentage of each scaffold was measured three times and the mean values were used for comparison. The samples did not show any toxic effects. The difference between the values obtained from scaffolds could be due to the amount of porosities in the scaffolds. Bhattarai et al [49] have shown that higher porosity end up with greater proliferation rate. Figure 9 shows that the cell proliferation was higher on 60% Mg than on 45 and 30% Mg in porous Ti-6Al-4V, in agreement with the observations of Li et al [50]. In sample with 64% porosity, cells migrates faster inside the pores of scaffold since pore space increased with porosity and facilitated transport of nutrients and oxygen. In fact higher porosity did not affect cell attachment, but resulted in increased cell proliferation. This observation has also been reported by Takahashi et al [51].

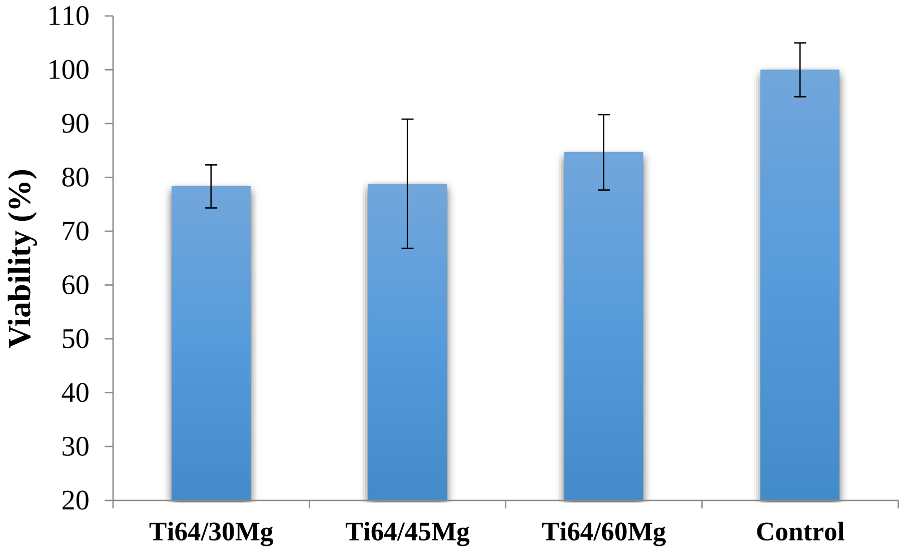

Fig 3.13 MG-63 cell proliferation on porous scaffolds after 7 days.

.

Chapter 4

Conclusion

Ti-6Al-4V scaffolds having various amounts of Mg elements within its composition were successfully fabricated by powder metallurgy technique. Partial evaporation of magnesium during sintering caused the formation of evenly distributed pores within the scaffold. The following conclusions are drawn:

1) Total and open porosities of the scaffolds were 46-63 vol.% and 41-47 vol.%, respectively. The degree of roundness of pores was within the range of 22-28%.
2) Two ranges of the pores were obtained; one in the range of 50-100μm and the other was several micrometers long. Therefore a bimodal distributing pore size was obtained which is suitable for application as biomaterials.
3) After immersion for 28 days in simulation body fluid, Calcium and phosphorus precipitated on the interior surfaces but more on pores surfaces. This shows the ability of scaffold to induce apatite nucleation and growth on these surfaces.
4) The pH values rose with increasing the mass fraction of magnesium. This increase can easily lead to decrease of HA solubility, and accordingly, a very large acceleration of apatite nucleation.
5) Deposition of Calcium and phosphorus in the porous areas was more than the smoother areas of the scaffold surfaces. This was attributed to higher presence of magnesium in porous areas resulting to more partial evaporation of Mg in these areas.
6) The compressive strength and elastic modulus of the porous samples decrease significantly with increasing the amount of Mg. Mechanical properties at the porosity of around 47 vol% are found to be with those of human cortical bone.

7) MG63 cells, with the diameter of 30 m, showed exert good stretching ability in the pores with the size of 30 m, inferring that the cells could migrate and settle into the pores with the size equal to itself.

References

[1]. J. Park, R. Lakes, Introduction to Biomaterials, Biomaterials, Springer US1992, pp. 1-6.

[2]. H. Hermawan, Introduction to Metallic Biomaterials, Biodegradable Metals, Springer2012, pp. 1-11

[3]. B. Arifvianto, J. Zhou, Fabrication of Metallic Biomedical Scaffolds with the Space Holder Method: A Review, Materials, 7 (2014) 3588-3622.

[4]. G. Ryan, P. McGarry, A. Pandit, D. Apatsidis, Analysis of the mechanical behavior of a titanium scaffold with a repeating unit-cell substructure, Journal of Biomedical Materials Research Part B: Applied Biomaterials, 90 (2009) 894-906.

[5]. Y. Oshida, Bioscience and bioengineering of titanium materials, Elsevier2010.

[6]. N. Ayda, M. Alam, M. Ravindranath, Corrosion in titanium dental implants: literature review, The Journal of Indian prosthodonic society, 5 (2005) 126-131.

[7]. S.N. Dezfuli, S. Sadrnezhaad, M. Shokrgozar, S. Bonakdar, Fabrication of biocompatible titanium scaffolds using space holder technique, Journal of Materials Science: Materials in Medicine, 23 (2012) 2483-2488.

[8]. J. Li, J. De Wijn, C. Van Blitterswijk, K. De Groot, Porous Ti6Al4V scaffolds directly fabricated by 3D fibre deposition technique: effect of nozzle diameter, Journal of Materials Science: Materials in Medicine, 16 (2005) 1159-1163.

[9]. G. Kotan, A.Ş. Bor, Production and characterization of high porosity Ti-6Al-4V foam by space holder technique in powder metallurgy, Turkish Journal of Engineering and Environmental Sciences, 31 (2009) 149-156.

[10]. G. Ryan, A. Pandit, D.P. Apatsidis, Fabrication methods of porous metals for use in orthopaedic applications, Biomaterials, 27 (2006) 2651-2670.

[11]. Y. Chen, B. Feng, Y. Zhu, J. Weng, J. Wang, X. Lu, Fabrication of porous titanium implants with biomechanical compatibility, Materials Letters, 63 (2009) 2659-2661.

[12]. S.W. Kim, H.-D. Jung, M.-H. Kang, H.-E. Kim, Y.-H. Koh, Y. Estrin, Fabrication of porous titanium scaffold with controlled porous structure and net-shape using magnesium as spacer, Materials Science and Engineering: C, 33 (2013) 2808-2815.

[13]. M. Niinomi, Mechanical properties of biomedical titanium alloys, Materials Science and Engineering: A, 243 (1998) 231-236.

[14]. X. Zhang, G. Zheng, J. Wang, Y. Zhang, G. Zhang, Z. Li, Y. Wang, Porous Ti6Al4V scaffold directly fabricated by sintering: preparation and in vivo experiment, Journal of Nanomaterials, 2013 (2013) 18.

[15]. L.M.R. de Vasconcellos, Y.R. Carvalho, R.F. do Prado, L.G.O. de Vasconcellos, M.L. de Alencastro Graça, C.A.A. Cairo, Porous Titanium by Powder Metallurgy for Biomedical Application: Characterization, Cell Citotoxity and in vivo Tests of Osseointegration, (2012).

[16]. A. Mansourighasri, N. Muhamad, A. Sulong, Processing titanium foams using tapioca starch as a space holder, Journal of Materials Processing Technology, 212 (2012) 83-89.

[17]. G. Kotan, A.Ş. Bor, Production and characterization of high porosity Ti-6Al-4V foam by space holder technique in powder metallurgy, Turkish Journal of Engineering and Environmental Sciences, 31 (2007) 149-156

[18]. N. Jha, D. Mondal, J. Dutta Majumdar, A. Badkul, A. Jha, A. Khare, Highly porous open cell Ti-foam using NaCl as temporary space holder through powder metallurgy route, Materials & Design, 47 (2013) 810-819.

[19]. O. Smorygo, A. Marukovich, V. Mikutski, A. Gokhale, G.J. Reddy, J.V. Kumar, High-porosity titanium foams by powder coated space holder compaction method, Materials Letters, 83 (2012) 17-19.

[20]. W.F. Ng, K.Y. Chiu, F.T. Cheng, Effect of pH on the in vitro corrosion rate of magnesium degradable implant material, Materials Science and Engineering: C, 30 (2010) 898-903.

[21]. R. Zeng, W. Dietzel, F. Witte, N. Hort, C. Blawert, Progress and challenge for magnesium alloys as biomaterials, Advanced Engineering Materials, 10 (2008) B3-B14.

[22]. H. Zreiqat, C. Howlett, A. Zannettino, P. Evans, G. Schulze-Tanzil, C. Knabe, M. Shakibaei, Mechanisms of magnesium-stimulated adhesion of osteoblastic cells to commonly used orthopaedic implants, Journal of biomedical materials research, 62 (2002) 175-184.

[23]. T. Aydoğmuş, Ş. Bor, Processing of porous TiNi alloys using magnesium as space holder, Journal of Alloys and Compounds, 478 (2009) 705-710.

[24]. A. Yamamoto, S. Hiromoto, Effect of inorganic salts, amino acids and proteins on the degradation of pure magnesium in vitro, Materials Science and Engineering: C, 29 (2009) 1559-1568.

[25]. M. Nan, C. Yangmei, Y. Bangcheng, Magnesium metal—A potential biomaterial with antibone cancer properties, Journal of Biomedical Materials Research Part A, (2013).

[26]. G. Song, Control of biodegradation of biocompatable magnesium alloys, Corrosion Science, 49 (2007) 1696-1701.

[27]. A. Mahboubi Soufiani, M. Enayati, F. Karimzadeh, Fabrication and characterization of nanostructured Ti6Al4V powder from machining scraps, Advanced Powder Technology, 21 (2010) 336-340.

[28]. A. F1580-01, Standard Specification for Titanium and Titanium-6 Aluminum-4 Vanadium Alloy Powders for Coatings of Surgical Implants.

[29]. T. Kokubo, H. Takadama, How useful is SBF in predicting in vivo bone bioactivity?, Biomaterials, 27 (2006) 2907-2915.

[30]. I.-H. Oh, N. Nomura, N. Masahashi, S. Hanada, Mechanical properties of porous titanium compacts prepared by powder sintering, Scripta Materialia, 49 (2003) 1197-1202.

[31]. J. Bobyn, J. Miller, Features of biologically fixed devices, orthopaedic basic science. Am Acad Orthop Surg, 10 (1994) 613-616.

[32]. A.I. Itälä, H.O. Ylänen, C. Ekholm, K.H. Karlsson, H.T. Aro, Pore diameter of more than 100 μm is not requisite for bone ingrowth in rabbits, Journal of biomedical materials research, 58 (2001) 679-683.

[33]. D.A. Robinson, R.W. Griffith, D. Shechtman, R.B. Evans, M.G. Conzemius, In vitro antibacterial properties of magnesium metal against Escherichia coli, Pseudomonas aeruginosa and Staphylococcus aureus, Acta biomaterialia, 6 (2010) 1869-1877.

[34]. A. Pietak, P. Mahoney, G.J. Dias, M.P. Staiger, Bone-like matrix formation on magnesium and magnesium alloys, Journal of Materials Science: Materials in Medicine, 19 (2008) 407-415.

[35]. M. Bohner, J. Lemaitre, Can bioactivity be tested in vitro with SBF solution?, Biomaterials, 30 (2009) 2175-2179.

[36]. H. Kuwahara, Y. Al-Abdullat, N. Mazaki, S. Tsutsumi, T. Aizawa, Precipitation of magnesium apatite on pure magnesium surface during immersing in Hank's solution, Materials Transactions(Japan), 42 (2001) 1317-1321.

[37]. L. Jonášová, F.A. Müller, A. Helebrant, J. Strnad, P. Greil, Biomimetic apatite formation on chemically treated titanium, Biomaterials, 25 (2004) 1187-1194.

[38]. S. Ibasco, F. Tamimi, R. Meszaros, D.L. Nihouannen, S. Vengallatore, E. Harvey, J.E. Barralet, Magnesium-sputtered titanium for the formation of bioactive coatings, Acta biomaterialia, 5 (2009) 2338-2347.

[39]. L. Xu, G. Yu, E. Zhang, F. Pan, K. Yang, In vivo corrosion behavior of Mg-Mn-Zn alloy for bone implant application, Journal of Biomedical Materials Research Part A, 83 (2007) 703-711.

[40]. G. Gagg, E. Ghassemieh, F.E. Wiria, Effects of sintering temperature on morphology and mechanical characteristics of 3D printed porous titanium used as dental implant, Materials Science and Engineering: C, 33 (2013) 3858-3864.

[41]. G. İpek Nakaş, A.F. Dericioglu, Ş. Bor, Fatigue behavior of TiNi foams processed by the magnesium space holder technique, Journal of the mechanical behavior of biomedical materials, 4 (2011) 2017-2023.

[42]. J. Umeda, M. Kawakami, K. Kondoh, E.-S. Ayman, H. Imai, Microstructural and mechanical properties of titanium particulate reinforced magnesium composite materials, Materials Chemistry and Physics, 123 (2010) 649-657.

[43]. A. Taşdemirci, A. Hızal, M. Altındiş, I. Hall, M. Güden, The effect of strain rate on the compressive deformation behavior of a sintered Ti6Al4V powder compact, Materials Science and Engineering: A, 474 (2008) 335-341

[44]. H. Zreiqat, C. Howlett, A. Zannettino, P. Evans, G. Schulze-Tanzil, C. Knabe, M. Shakibaei, Mechanisms of magnesium-stimulated adhesion of osteoblastic cells to commonly used orthopaedic implants, Journal of biomedical materials research, 62 (2002) 175-184.

[45]. K. Anselme, Osteoblast adhesion on biomaterials, Biomaterials, 21 (2000) 667-681.

[46]. J. Chen, E. Paetzell, J. Zhou, L. Lyons, W. Soboyejo, Osteoblast-like cell ingrowth, adhesion and proliferation on porous Ti-6Al-4V with particulate and fiber scaffolds, Materials Science and Engineering: C, 30 (2010) 647-656.

[47]. W. Xue, B.V. Krishna, A. Bandyopadhyay, S. Bose, Processing and biocompatibility evaluation of laser processed porous titanium, Acta Biomaterialia, 3 (2007) 1007-1018.

[48]. Y. Tian, S. Ding, H. Peng, S. Lu, G. Wang, L. Xia, P. Wang, Osteoblast growth behavior on porous-structure titanium surface, Applied Surface Science, 261 (2012) 25-30.

[49]. S.R. Bhattarai, K.A.R. Khalil, M. Dewidar, P.H. Hwang, H.K. Yi, H.Y. Kim, Novel production method and in-vitro cell compatibility of porous Ti-6Al-4V alloy disk for hard tissue engineering, Journal of Biomedical Materials Research Part A, 86 (2008) 289-299.

[50]. J.P. Li, P. Habibovic, M. van den Doel, C.E. Wilson, J.R. de Wijn, C.A. van Blitterswijk, K. de Groot, Bone ingrowth in porous titanium implants produced by 3D fiber deposition, Biomaterials, 28 (2007) 2810-2820.

[51]. Y. Takahashi, Y. Tabata, Effect of the fiber diameter and porosity of non-woven PET fabrics on the osteogenic differentiation of mesenchymal stem cells, Journal of Biomaterials Science, Polymer Edition, 15 (2004) 41-57.